Taming Metal-Organic Framework (MOF)-Based Luminescence Sensing through Open-Metal Site Regulation

Zongsu Han,[1,§] Yifan Guo,[2,§] Rongran Liang,[1,§] Kun-Yu Wang,[1,*] Yihao Yang,[1] Mengmeng Wang,[4] Yann Garcia,[4] Peter R. Taylor,[2] Wei Shi,[3,*] and Hong-Cai Zhou[1,*]

[1]Department of Chemistry, Texas A&M University, College Station, Texas 77843, United States. [2]Health Science Platform, Tianjin University, A203, Bldg. 24, 92 Weijin Rd., Nankai Dist., Tianjin 300072, China. [3]Frontiers Science Center for New Organic Matter, Key Laboratory of Advanced Energy Materials Chemistry (MOE), and State Key Laboratory of Advanced Chemical Power Sources, College of Chemistry, Nankai University, Tianjin 300071, China. [4]Institute of Condensed Matter and Nanosciences, Molecular Chemistry, Materials and Catalysis (IMCN/MOST), Université catholique de Louvain, 1348 Louvain-la-Neuve, Belgium. Correspondence and requests for materials should be addressed to H.-C. Z. (email: zhou@chem.tamu.edu)

ABSTRACT

Open metal sites (OMSs) represent a distinctive feature of metal–organic frameworks (MOFs), intertwined with guest accommodation and energy transfer within nanosized pores. Fine-tuning OMSs provide an effective approach to regulating MOF's responsiveness and binding affinity towards guests, allowing for the construction of luminescent sensors for specific analytes. Such a strategy remains unexplored due to the inherent complexity of the systems and sensing mechanisms. Herein, we delicately regulated the OMSs in PCN-700 through multiple synthetic methodologies. The resultant MOFs consist of Zr_6-clusters featuring various coordination numbers. Notably, PCN-700-8u with unsaturated 8-coordinated Zr-clusters exhibited the highest sensitivity in detecting pentachloronitrobenzene due to the presence of coordination interaction, as validated through single crystal X-ray diffraction. Additionally, PCN-700-10u/12u bearing unsaturated 10/12-coordinated clusters perform lower quenching efficiencies than PCN-700-8u, but higher than PCN-700-12s with saturated clusters. Besides, all these MOFs perform similar quenching efficiencies towards hexachlorobenzene for the absence of coordination interaction. This study not only develops a cost-effective and easily-attainable material for pentachloronitrobenzene detection, but also illuminates the pivotal importance of OMSs in customizing MOF-based sensors for practical requirements.

Introduction

Given the advancement in agricultural techniques, the widespread application of pesticides and insecticides has become increasingly pivotal in modern society and production. However, these chemicals can be preserved within soil and water bodies for years, posing significant threats to public health and safety.[1,2] Certain pesticides and insecticides are even known to exhibit carcinogenic properties.[3,4] Pentachloronitrobenzene (PCNB), an organochlorine fungicide primarily utilized in soil and seed treatment, has been globally applied for many years. Unfortunately, recent reports indicate the potential toxicity of PCNB towards both crops and mammals, raising concerns about its potential carcinogenic effects on humans.[5,6] Hexachlorobenzene (HCB), a byproduct stemming from PCNB production, previously utilized as a pesticide, has been categorized as persistent organic pollutants in the Stockholm Convention due to its substantial toxicity.[7,8] Hence,

the development of an effective and real-time sensing method for PCNB has become imperative for detecting environmental residues and ensuring the pesticide's purity. Considering the structural characteristics, the nitro group present in PCNB demonstrates the ability for coordination, thereby indicating its plausibility to be recognized.

Open metal site (OMS) represents a significant feature of metal–organic frameworks (MOFs), particularly while combined with nanosized pores, showcasing remarkable properties for a wide array of applications, such as gas storage, selective separation, and catalysis.[9-13] Luminescent sensing has been recognized as an effective sensing method for various analytes, including metal ions, solvents, volatile organic compounds, persistent organic pollutants, and biomarkers.[14-20] Nevertheless, the impact of the OMS within MOF-based luminescent sensors remains largely untapped, especially the numbers of the OMSs, due to the grand challenge of constructing MOFs with similar framework structures by identical ligands and metal clusters, while the sensing mechanisms are really complicated with severe interference. PCN-700 stands out as a unique MOF assembled by an 8-connected unsaturated Zr_6 cluster, bearing a highly flexible structure.[21] The dense OMSs on the cluster, coupled with the framework's flexibility, enable the incorporation ligands with diverse lengths into this MOF, thereby facilitating multiple functions like sensing and catalysis.[22,23] Moreover, PCN-700 features two distinct "pockets" with 7.0 Å and 16.4 Å in diameter, capable of accommodating varied molecules.[21-23]

In this study, a series of PCN-700 analogues with varied topologies were constructed using the same H_2Me_2-BPDC ligand (H_2Me_2-BPDC = 2,2'-dimethylbiphenyl-4,4'-dicarboxylic acid) and Zr_6 cluster. For clarity, the PCN-700 analogues are labelled as 8u, 10u, 12u, and 12s, respectively, wherein the number refers to the coordination number of the Zr-cluster and u/s stands for unsaturation/saturation coordination of Zr_6-oxo clusters. PCN-700-8u and PCN-700-10u were generated through direct synthesis at different temperatures, resulting in the formation of 8-connected and 10-connected unsaturated Zr_6-clusters, with OMSs 1 and 2, and OMS 2, respectively. Employing the linker installation method on PCN-700-8u led to the construction of PCN-700-12u, yielding a 12-connected unsaturated Zr_6-oxo cluster, with OMS 2 only. Besides, PCN-700-12s was obtained via linker exchange performed on UiO-67, resulting in a 12-connected saturated Zr_6-cluster. Among these four MOFs, the PCN-700-8u with the densest OMSs exhibited the highest quenching efficiency towards PCNB. Additionally, compared to sensing the uncoordinated molecule HCB, PCN-700-8u displayed superior sensing efficiency towards PCNB, underscoring the impact of coordination interactions on the MOF's sensing performance. Also, other unsaturation MOFs PCN-700-10u and PCN-700-12u with the same amount of OMSs possess similar quenching efficiencies towards PCNB, and higher than the saturated PCN-700-12s. All these four MOFs possess similar quenching efficiencies towards HCB (Fig. 1). Notably, the coordination interaction between PCN-700-8u and PCNB was revealed through single crystal X-ray diffraction, indicating the highly ordered binding sites.

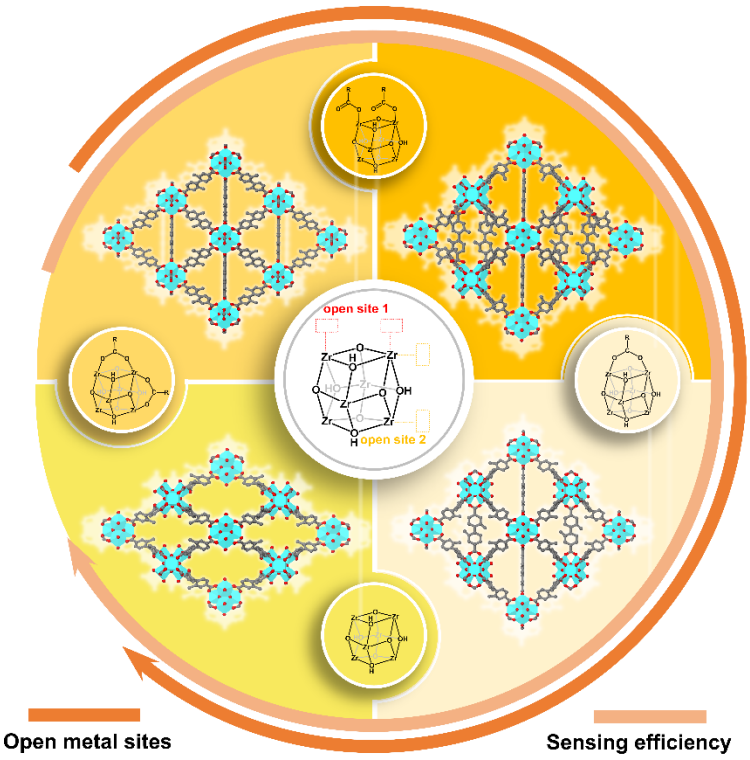

Figure 1. Overview scheme. The interactions between the numbers of the open metal sites and sensing efficiency towards PCNB based on PCN-700 series.

Results

Structure and basic characterization

Pristine PCN-700-8u crystals were synthesized using $ZrCl_4$ and H_2Me_2-BPDC under 120 °C, in which the Zr_6 cluster was connected with 8 ligands to form a highly flexible framework featuring ~14.7 Å at the *c* axis. When increasing the synthetic temperature to 140 °C, PCN-700-10u crystals can be obtained with one additional Me_2-BPDC occupying the small pocket of PCN-700-8u, wherein each Zr_6 cluster was connected with 10 ligands to elongate the *c* axis to ~19.0 Å. In addition, PCN-700-8u crystals can be used as the raw materials for the linker installation of H_2Me_2-BPDC to form PCN-700-12u with ~18.9 Å in *c* axis. Two Me_2-BPDC ligands were found in the same small pocket, leading to 12-connected Zr_6 clusters and open large pockets. Besides, UiO-67 crystals were synthesized by using H_2BPDC (H_2BPDC = biphenyl-4,4'-dicarboxylic acid) under the similar conditions as PCN-700-8u. Then H_2Me_2-BPDC was subsequently used to replace the BPDC linker through linker exchange to obtain PCN-700-12s, in which each Zr_6 cluster was saturated with 12 ligands, bearing a *c* axis of ~26.8 Å (Fig. 2 and Supplementary Table 1).

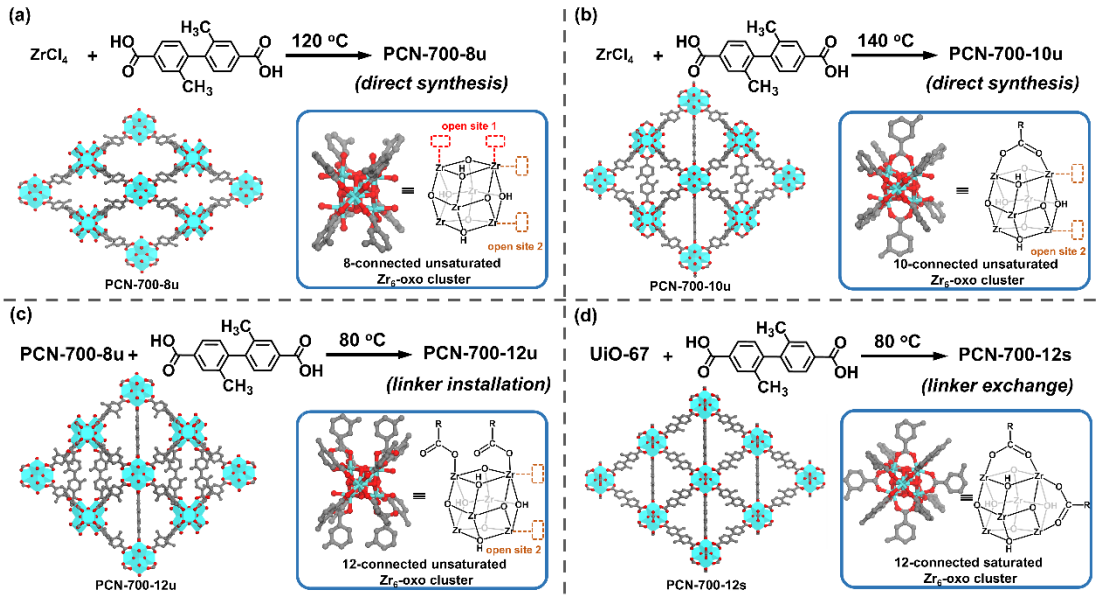

Figure 2. Synthetic procedures and structural illustrations. (a) PCN-700-8u. (b) PCN-700-10u. (c) PCN-700-12u. (d) PCN-700-12s.

The phase purities of all aforementioned MOFs were confirmed by powder X-ray diffraction (PXRD) patterns (Supplementary Fig. 1) and infrared (IR) spectroscopy (Supplementary Fig. 2). Thermogravimetry analysis was also performed to show the thermal stability (Supplementary Fig. 3). ^{1}H nuclear magnetic resonance (NMR) spectra were used to identify the linker exchange ratio in UiO-67 (Supplementary Fig. 4), indicating that ~60% BPDC ligands have been exchanged. Ultraviolet–visible (UV-vis) spectroscopy (Supplementary Fig. 5) and emission spectra (Supplementary Fig. 6) of these MOFs were collected when dispersed in *N*,*N*-dimethylformamide (DMF), demonstrating obvious differences in intensities, especially for PCN-700-12u, which may be attributed to the end-vibration-induced energy dissipation.[24]

Luminescence sensing

Inspired by the structural difference in topologies and open sites of the as-synthesized PCN-700 analogues, systematic studies were conducted to elucidate their potential in luminescence sensing. Firstly, to study the sensing functions of PCN-700, time-dependent luminescence intensities of PCN-700 in DMF were first recorded and kept stable (Supplementary Fig. 7), demonstrating the minimal time interference. Response time of PCN-700 towards PCNB was also measured, while the intensities could remain stable within ten seconds (Supplementary Fig. 8), confirming the rapid response ability.

Furthermore, PCNB at the same concentration was added dropwise to these four MOFs, respectively, while distinct decrease in luminescence intensities was observed (Supplementary Fig. 9-12). In particular, the emission intensities originated from the ligand at ~350 nm show different quenching efficiencies in these MOFs (Fig. 3a). The luminescence quenching efficiency at low concentrations can be quantitatively described by the linear Stern–Volmer (S–V) equation (Supplementary Fig. 9-12), $I_0/I = K_{SV}[C] + b$,[25-27] where K_{SV} is the quenching constant (M^{-1}), C is the concentration of the added PCNB, b is a constant, and I_0 and I are the luminescence intensities before and after the analyte additions, respectively. When the concentration of PCNB increased, the

luminescence intensity curve of PCN-700-10u gradually deviated from linear and bent upward, which can be fitted by the exponential nonlinear S–V equation I_0/I = a exp(k[C]) + b,[28-30] where a, b, and k are constants. From the results, PCN-700-8u, with the most abundant OMSs, features the best sensitivity towards PCNB with a 7.18 × 10^3 M^{-1} K_{SV} value. PCN-700-10u and PCN-700-12u with the same OMSs possessing similar K_{SV} values, which are higher than the saturated PCN-700-12s (Fig. 3b).

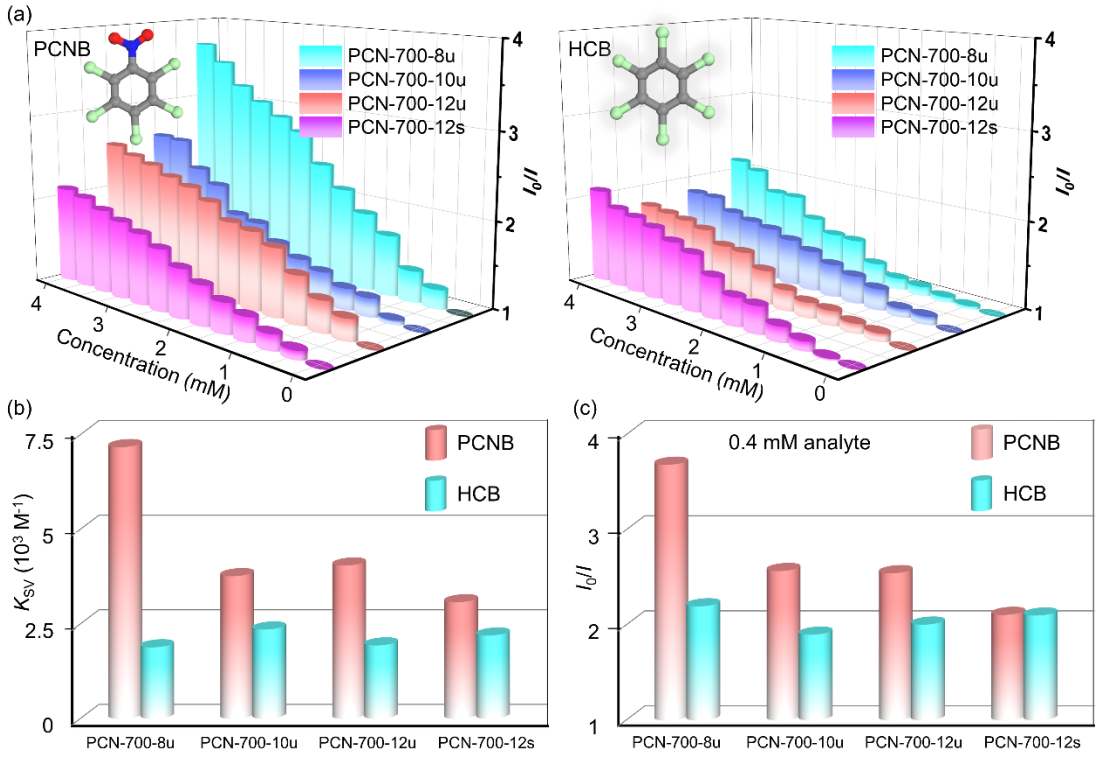

Figure 3. Sensing results. (a) Emission intensity changes of PCN-700-8u, PCN-700-10u, PCN-700-12u, and PCN-700-12s towards additions of PCNB and HCB. (b) Comparisons of the K_{SV} values of PCN-700-8u, PCN-700-10u, PCN-700-12u, and PCN-700-12s. (c) Comparisons of the intensity changes of PCN-700-8u, PCN-700-10u, PCN-700-12u, and PCN-700-12s with additions of 0.4 mM PCNB and HCB.

To further understand the contribution of the OMSs to sensing, the common by-product of PCNB, HCB, was selected for comparison (Fig. 3). Compared to PCNB, the nitro group was replaced by one chlorine atom in HCB. Following a similar process as the sensing experiment towards PCNB, the same concentration of HCB was added dropwise to these MOFs respectively, while the luminescence intensities were recorded (Supplementary Fig. 13-16). The luminescence quenching efficiency at low concentrations can be quantitatively described by the linear S–V equation (Supplementary Fig. 13-16). From the results, PCN-700-8u features better sensitivity towards PCNB than HCB, highlighting the significance of OMSs in sensing (Fig. 3b). Meanwhile, the quenching of unsaturated PCN-700-10u and PCN-700-12u towards HCB is weaker than the ones towards PCNB (Fig. 3c), which further confirms the significance of OMSs.

Underlying mechanism

In order to fully uncover the sensing mechanism within PCN-700-8u in detail, single crystal X-ray diffraction data were collected. The crystal structure of PCNB-loaded PCN-700-8u was resolved, indicating that the PCNB was present on the OMSs of the Zr-cluster in the small pocket (Fig. 4 and Supplementary Table 1). While for the other three MOFs, the small pockets have already been occupied by the ligand, impeding the accommodation of PCNB. To confirm the successful loading of PCNB, the PCNB-loaded PCN-700-8u was decomposed using d_6-DMSO (DMSO = dimethyl sulfoxide) and D_2SO_4 to collect ^{13}C NMR spectrum, which shows the peaks of PCNB (Supplementary Fig. 17). In addition, density functional theory (DFT) calculation was conducted to evaluate the binding energy of PCNB towards PCN-700-8u analogues (Supplementary Fig. 18), which further confirms the strong interactions between PCN-700-8u with PCNB.

Figure 4. Structure changes for PCN-700-8u with PCNB. Framewrok structure changes of PCN-700-8u with the additions of PCNB, detected by single crystal X-ray diffraction.

Other characterizations and analyses were carried out to further explain the sensing mechanisms. PXRD patterns and IR spectra of the MOFs remain the same after the sensing experiments (Supplementary Fig. 19), indicating that the sensing performance was not induced by the structure transforms or framework collapses. Furthermore, there are overlaps between the UV-vis absorption spectra of PCNB/HCB and MOFs dispersed in DMF, which demonstrates the competitive absorption (CA) of the excitation energy, leading to decreased emission intensity (Fig. 5). For the emission energy, there are overlaps between the absorption spectra of PCNB and the emission spectra of the MOF dispersions in DMF, but no obvious overlaps are observed for HCB, which indicates the presence of the Förster resonance energy transfer (FRET) process towards PCNB, and absence towards HCB (Fig. 5).[31,32] Such a sensing mechanism may lead to the lower quenching efficiencies of these MOFs towards HCB compared with PCNB.

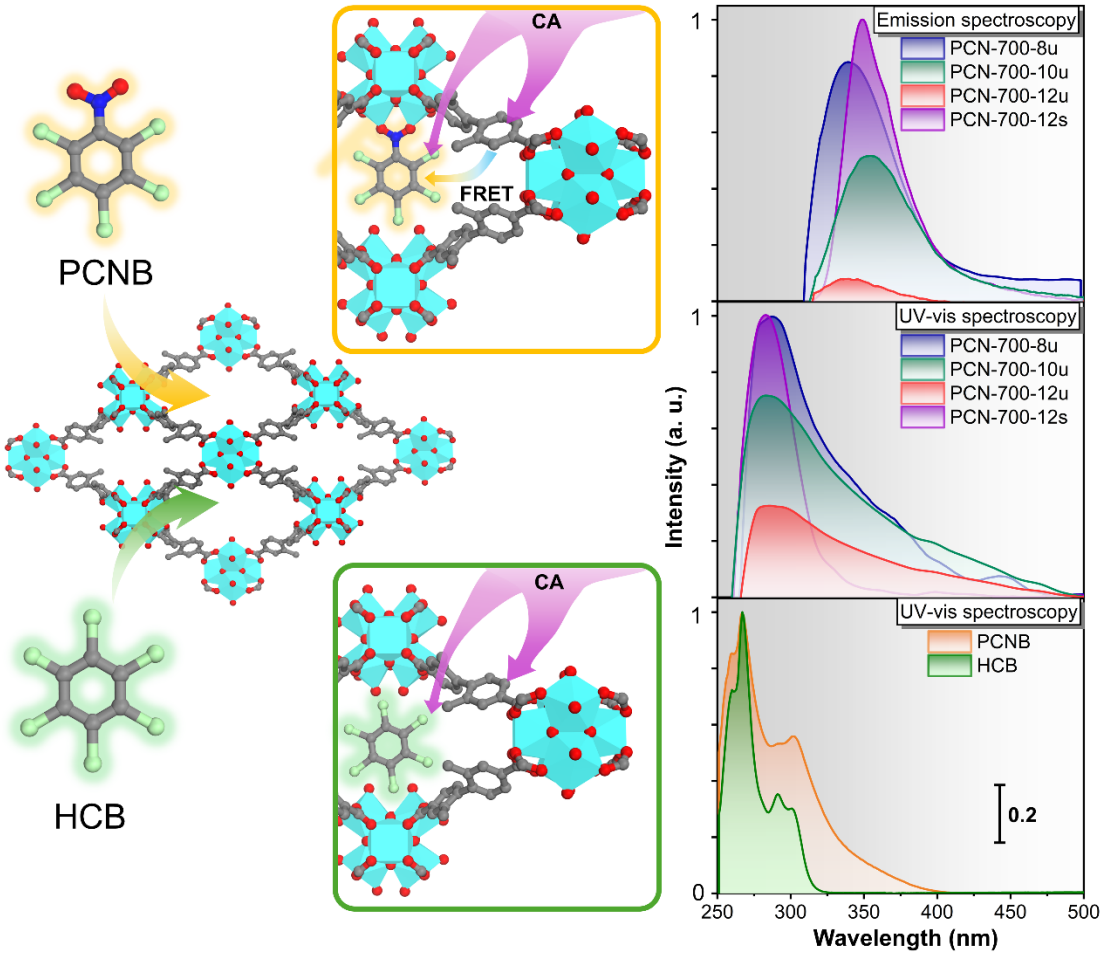

Figure 5. Sensing mechanisms. Sensing mechanisms of PCN-700 towards PCNB and HCB with the corresponding emission spectra and UV-vis spectra.

Discussion

In summary, this research successfully constructed four Zr_6-cluster-based MOFs through direct synthesis, ligand installation, and ligand exchange processes, to construct a series of MOFs with similar framework structures. These methods facilitated the development of metal clusters with diverse coordination numbers and OMSs by using the same organic ligands and metal atoms. The varied OMSs are pivotal to affect the sensing performance of these Zr-based MOFs towards analytes containing coordinative functional groups, a characteristic not observed in analytes lacking these groups, confirmed by toxic pesticides PCNB and HCB. This study not only enriched the synthetic toolkit of Zr-based MOFs but also uncovered the significant role of the density of OMSs in MOF-based luminescent sensing, shedding light on constructing efficient sensing materials with atomic precision.

Methods

Materials and Methods

All reagents were commercially available and used without further purification. Liquid ^{1}H NMR and ^{13}C NMR spectra were recorded on a Bruker Avance NEO 400 NMR spectrometer. Single crystal X-ray diffraction patterns were collected by a Bruker-Axs Venture Ius Cmos Kappa X-ray Apex2 diffractometer with Cu-Kα radiation and a Bruker-Axs Quest Ius Three-Circle X-ray Apex2

diffractometer with Mo-Kα radiation. PXRD measurements were performed using a Bruker Powder-ECO X-ray diffractometer with Cu-Kα radiation. Thermo-gravimetric analysis curves were obtained under nitrogen atmosphere on a Mettler Toledo TGA/DSC 1 thermogravimetric analyzer from 40 °C to 800 °C. Luminescence spectra were recorded on a Shimadzu RF-5301 fluorescence spectrophotometer. UV-vis absorption spectra were measured by a Shimadzu UV-2450 Spectrometer. IR spectra were tested by a Shimadzu IRAffinity-1 spectrometer. 3 mg MOFs for NMR tests were dissolved by 0.5 mL d_6-DMSO and 5 μL D_2SO_4.

Synthesis

PCN-700-8u and UiO-67 were synthesized according to the literature.[33]

Synthesis of PCN-700-10u.

$ZrCl_4$ 20 mg, H_2Me_2-BPDC 10 mg, trifluoroacetic acid 0.1 mL were solved in 2 mL DMF and charged in a Pyrex vial. The mixture was heated in 140 ºC oven for 3 days. The crystals were collected by filtration, washed with fresh DMF, and soaked in fresh DMF for night.

Synthesis of PCN-700-12u.

10 mg PCN-700 was treated with the solution of 20 mg H_2Me_2-BPDC in 10 mL DMF at 80 ºC for 3 days. Then the crystals were collected by filtration, washed with fresh DMF, and soaked in fresh DMF for night.

Synthesis of PCN-700-12s.

10 mg UiO-67 was treated with the solution of 20 mg H_2Me_2-BPDC in 10 mL DMF at 80 ºC for 7 days. Then the crystals were collected by filtration, washed with fresh DMF, and soaked in fresh DMF for night.

Luminescence experiments

All samples were grinded into fine powder before use. The samples for luminescence experiments were dispersed in DMF by ultrasound for 10 minutes to form a clear suspension with a concentration of 0.3 mg mL^{-1}. PCNB and HCB were diluted by DMF with a concentration of 0.3 mg mL^{-1}, which were further added to the MOF suspension. Each line was tested after 10 seconds ultrasound. All the emission spectra were excited under 300 nm.

Data Availability

The data that support the findings of this study are available from the corresponding author.

References

1. Rodrigo, M. A., Oturan, N., Oturan, M. A. Electrochemically assisted remediation of pesticides in soils and water: a review. *Chem. Rev.* **114**, 8720-8745 (2014).
2. Möhring, N., Ingold, K., Kudsk, P., Martin-Laurent, F., Niggli, U., Siegrist, M., Studer, B., Walter, A., Finger, R. Pathways for advancing pesticide policies. *Nat. Food* **1**, 535-540 (2020).
3. Alavanja, M. C. R., Ross, M. K., Bonner, M. R. Increased cancer burden among pesticide applicators and others due to pesticide exposure. *CA-Cancer J. Clin*. **63**, 120-142 (2013).

4. Gatto, N. M., Ogata, P., Lytle, B. Farming, pesticides, and brain cancer: a 20-year updated systematic literature review and meta-analysis. *Cancers* **13**, 4477 (2021).
5. Tas, D. O., Pavlostathis, S. G. Occurrence, toxicity, and biotransformation of pentachloronitrobenzene and chloroanilines. *Crit. Rev. Environ. Sci. Technol.* **44**, 473-518 (2014).
6. Fan, G., Shen, T., Jia, K., Xiao, X., Wu, Z., Gong, F., Lu, H. Pentachloronitrobenzene reduces the proliferative capacity of zebrafish embryonic cardiomyocytes via oxidative stress. *Toxics* **10**, 299 (2022).
7. Tu, Z., Qi, Y., Qu, R., Tang, X., Wang, Z., Huo, Z. Photochemical transformation of hexachlorobenzene (HCB) in solid-water system: Kinetics, mechanism and toxicity evaluation. *Chemosphere* **295**, 133907 (2022).
8. Sun, W., Jia, Y., Ding, X., Dai, L., Liu, C., Wang, J., Zhao, G., Zhou, H., Yu, L. Combined effects of pentachlorophenol and its byproduct hexachlorobenzene on endocrine and reproduction in zebrafish. *Chemosphere* **220**, 216-226 (2019).
9. Niu, Z., Cui, X., Pham, T., Verma, G., Lan, P. C., Shan, C., Xing, H., Forrest, K. A., Suepaul, S., Space, B., Nafady, A., Al-Enizi, A. M., Ma, S. A MOF-based ultra-strong acetylene nano-trap for highly efficient C_2H_2/CO_2 separation. *Angew. Chem. Int. Ed*. **60**, 5283-5288 (2021).
10. Zeng, H., Xie, M., Huang, Y. L., Zhao, Y., Xie, X. J., Bai, J. P., Wan, M. Y., Krishna, R., Lu, W., Li, D. Induced fit of C_2H_2 in a flexible MOF through cooperative action of open metal sites. *Angew. Chem. Int. Ed*. **58**, 8515-8519 (2019).
11. Kökçam-Demir, Ü., Goldman, A., Esrafili, L., Gharib, M., Morsali, A., Weingart, O., Janiak, C. Coordinatively unsaturated metal sites (open metal sites) in metal–organic frameworks: design and applications. *Chem. Soc. Rev*. **49**, 2751-2798 (2020).
12. Zhang, C., Shen, L., Shen, J., Liu, F., Chen, G., Tao, R., Ma, S., Peng, Y., Lu, Y. Anion-sorbent composite separators for high-rate lithium-ion batteries. *Adv. Mater.* **31**, 1808338 (2019).
13. Britt, D., Furukawa, H., Wang, B., Glover, T. G., Yaghi, O. M. Highly efficient separation of carbon dioxide by a metal-organic framework replete with open metal sites. *Proc. Natl. Acad. Sci.* **106**, 20637-20640 (2009).
14. Fu, J. H., Zhong, Z., Xie, D., Guo, Y. J., Kong, D. X., Zhao, Z. X., Zhao, Z. X., Li, M. SERS-active MIL-100 (Fe) sensory array for ultrasensitive and multiplex detection of VOCs. *Angew. Chem. Int. Ed.* **59**, 20489-20498 (2020).
15. Dong, M. J., Zhao, M., Ou, S., Zou, C., Wu, C. D. A luminescent dye@ MOF platform: emission fingerprint relationships of volatile organic molecules. *Angew. Chem. Int. Ed*. **53**, 1575-1579 (2014).
16. Chen, J., Zhu, Y., Kaskel, S. Porphyrin-based metal-organic frameworks for biomedical applications. *Angew. Chem. Int. Ed.* **60**, 5010-5035 (2021).
17. Gutiérrez, M., Zhang, Y., Tan, J. C. Confinement of luminescent guests in metal–organic frameworks: understanding pathways from synthesis and multimodal characterization to potential applications of LG@MOF systems. *Chem. Rev*. **122**, 10438-10483 (2022).
18. Li, Y., Yang, Z., Wang, Y., Bai, Z., Zheng, T., Dai, X., Liu, S., Gui, D., Liu, W., Chen, M., Chen, L., Diwu, J., Zhu, L., Zhou, R., Chai, Z., Albrecht-Schmitt, T. E., Wang, S. A mesoporous cationic thorium-organic framework that rapidly traps anionic persistent organic pollutants. *Nature Commun.* **8**, 1354 (2017).

19. Lustig, W. P., Mukherjee, S., Rudd, N. D., Desai, A. V., Li, J., Ghosh, S. K. Metal–organic frameworks: functional luminescent and photonic materials for sensing applications. *Chem. Soc. Rev*. **46**, 3242-3285 (2017).
20. Han, Z., Wang, K., Min, H., Xu, J., Shi, W., Cheng, P. Bifunctionalized metal-organic frameworks for pore-size-dependent enantioselective sensing. *Angew. Chem. Int. Ed.* **61**, e202204066 (2022).
21. Yuan, S., Lu, W., Chen, Y. P., Zhang, Q., Liu, T. F., Feng, D., Wang, X., Qin, J., Zhou, H. C. Sequential linker installation: precise placement of functional groups in multivariate metal–organic frameworks. *J. Am. Chem. Soc*. **137**, 3177-3180 (2015).
22. Yuan, S., Zou, L., Li, H., Chen, Y. P., Qin, J., Zhang, Q., Lu, W., Hall, M. B., Zhou, H. C. Flexible zirconium metal-organic frameworks as bioinspired switchable catalysts. *Angew. Chem. Int. Ed.* **55**, 10776-10780 (2016).
23. Li, J., Yuan, S., Qin, J. S., Pang, J., Zhang, P., Zhang, Y., Huang, Y., Drake, H. F., Liu, W. R., Zhou, H. C. Stepwise assembly of turn-on fluorescence sensors in multicomponent metal-organic frameworks for in vitro cyanide detection. *Angew. Chem. Int. Ed.* **59**, 9319-9323 (2020).
24. Zych, E. On the reasons for low luminescence efficiency in combustion-made Lu_2O_3: Tb. *Opt. Mater.* **16**, 445-452 (2001).
25. Hu, Z., Lustig, W. P., Zhang, J., Zheng, C., Wang, H., Teat, S. J., Gong, Q., Rudd, N. D., Li, J. Effective detection of mycotoxins by a highly luminescent metal–organic framework. *J. Am. Chem. Soc.* **137**, 16209-16215 (2015).
26. Wei, W., Lu, R. J., Tang, S. Y., Liu, X. Y. Highly cross-linked fluorescent poly (cyclotriphosphazene-co-curcumin) microspheres for the selective detection of picric acid in solution phase. *J. Mater. Chem. A* **3**, 4604-4611 (2015).
27. Wu, S., Lin, Y., Liu, J., Shi, W., Yang, G., Cheng, P. Rapid detection of the biomarkers for carcinoid tumors by a water stable luminescent lanthanide metal–organic framework sensor. *Adv. Funct. Mater.* **28**, 1707169 (2018).
28. Dinda, D., Gupta, A., Shaw, B. K., Sadhu, S., Saha, S. K. Highly selective detection of trinitrophenol by luminescent functionalized reduced graphene oxide through FRET mechanism. *ACS Appl. Mater. Interfaces* **6**, 10722-10728 (2014).
29. Han, Z., Wang, K., Zhou, H. C., Cheng, P., Shi, W. Preparation and quantitative analysis of multicenter luminescence materials for sensing function. *Nat. Protoc*. **18**, 1621-1640 (2023).
30. Han, Z., Wang, K., Guo, Y., Chen, W., Zhang, J., Zhang, X., Siligardi, G., Yang, S., Zhou, Z., Sun, P., Shi, W., Cheng, P. Cation-induced chirality in a bifunctional metal-organic framework for quantitative enantioselective recognition. *Nature Commun*. **10**, 5117 (2019).
31. Zhao, Y., Zeng, H., Zhu, X. W., Lu, W., Li, D. Metal–organic frameworks as photoluminescent biosensing platforms: mechanisms and applications. *Chem. Soc. Rev.* **50**, 4484-4513 (2021).
32. Razavi, S. A. A., Morsali, A. Metal ion detection using luminescent-MOFs: Principles, strategies and roadmap. *Coord. Chem. Rev.* **415**, 213299 (2020).
33. Yuan, S., Chen, Y. P., Qin, J. S., Lu, W., Zou, L., Zhang, Q., Wang, X., Sun, X., Zhou, H. C. Linker installation: engineering pore environment with precisely placed functionalities in zirconium MOFs. *J. Am. Chem. Soc.* **138**, 8912-8919 (2016).

Acknowledgments

This work was partially supported by the Robert A. Welch Foundation through an endowed chair (A-0030) to H.-C. Z. and National Natural Science Foundation of China (Grant Nos. 92156002, 21931004 and 22261132509). We thank the Fonds de la Recherche Scientifique-FNRS (PDR T.0095.21, FC 53249).

Author contributions

Z. H. did the main experiment, collected and interpreted the data. Y. G. and P. R. T. carried out the calculations. R. L., K.-Y. W., Y. Y., M. W., Y. G. and W. S. interpreted some data, figures, and the manuscript writing. H.-C. Z. mastered the whole experiment.

Additional information

Competing interests: The authors declare no competing interests.